AJNR

Proton MR Spectroscopy of Gliomatosis Cerebri: Case Report of Elevated Myoinositol with Normal Choline Levels

Efrat Saraf-Lavi, Brian C. Bowen, Pradip M. Pattany, Evelyn M.L. Sklar, James B. Murdoch and Carol K. Petito

AJNR Am J Neuroradiol 2003, 24 (5) 946-951
http://www.ajnr.org/content/24/5/946

AJNR Am J Neuroradiol 24:946–951, May 2003

Case Report

Proton MR Spectroscopy of Gliomatosis Cerebri: Case Report of Elevated Myoinositol with Normal Choline Levels

Efrat Saraf-Lavi, Brian C. Bowen, Pradip M. Pattany, Evelyn M.L. Sklar, James B. Murdoch, and Carol K. Petito

Summary: A 69-year-old woman presented with clinical and imaging findings suspicious for gliomatosis cerebri, later confirmed by biopsy (moderately cellular, infiltrating glioma). Single voxel proton MR spectroscopy (TE 20 and TE 135) and spectroscopic imaging (TE 135) performed at admission showed normal choline, decreased *N*-acetyl, and elevated *myo*-inositol levels relative to creatine. The primary conclusion is that in suspected cases of gliomatosis cerebri, *myo*-inositol/creatine and *myo*-inositol/*N*-acetyl should be determined because they may provide evidence of tumor, even though choline/creatine is normal. A corollary to this conclusion is that choline/creatine may be misleading if used to demarcate infiltrating glioma from edema.

Gliomatosis cerebri is characterized by contiguous involvement of at least two lobes of the brain by a glial cell tumor of neuroepithelial origin, with relative preservation of neuronal architecture (1). The unusually diffuse infiltration is predominantly along myelinated pathways. Features such as vascular proliferation and necrosis are typically absent. The diagnosis is usually made on the basis of both histology and neuroimaging. Conventional MR imaging shows a diffuse signal intensity abnormality with minimal or no mass effect and a lack of contrast enhancement. Although the clinical and MR imaging findings may suggest infiltrative neoplasm, they are not specific, and the use of proton MR spectroscopy to aid in classification of gliomatosis cerebri has been suggested (2). Two series of patients with proved gliomatosis cerebri who were evaluated with in vivo MR spectroscopic imaging, using TE 135 (2) or TE 144 (3), have been reported. In both series, choline (Cho)/creatine (Cr) values were elevated within brain areas that were hyperintense on T2-weighted or fluid-attenuated inversion recovery (FLAIR) images, compared with Cho/Cr values from normal appearing brain areas. In two case reports, investigators using single voxel proton MR spectroscopy (TE 30) but not MR spectroscopic imaging found normal Cho/Cr and either an elevated (4) or normal (5) resonance at 3.5 to 3.6 ppm (assigned to *myo*-inositol [*m*-Ins] and glycine [Gly]) relative to Cr, within hyperintense brain areas in three patients with gliomatosis cerebri. For the case reported herein, single voxel proton MR spectroscopy and MR spectroscopic imaging results are presented and show evidence of normal Cho/Cr and elevated *m*-Ins/Cr within hyperintense areas compared with values from normal appearing areas of the patient's brain and compared with corresponding areas of the brains of healthy volunteers.

Received August 12, 2002; accepted after revision September 11.

From the Departments of Radiology (E.S.-L., B.C.B., P.M.P., E.M.L.S.) and Pathology (C.K.P.), University of Miami School of Medicine, Miami, FL, and Philips Medical Systems (J.B.M.), Cleveland OH.

Address reprint requests to Brian C. Bowen, MD, PhD, Department of Radiology, University of Miami School of Medicine, 1115 NW 14th Street, Miami, FL 33135.

Case Report

A 69-year-old woman was admitted to our hospital with a 5-month history of progressive memory loss, personality change, right hand tremor, right-sided weakness, and fatigue. The patient also had experienced an episode of gait imbalance. Her medical history was positive for hypertension, hyperlipidemia, and coronary artery disease and was negative for stroke, transient ischemic attack, chronic infection, or other chronic illness. A physical examination revealed right pronator drift. The motor strength was intact, and no sensory deficits were detected. Babinski sign was absent. Blood count, biochemical profile, sedimentation rate, coagulation profile, and the results of radiography of the chest were normal. CSF analysis showed a red blood cell count of 1430, a white blood cell count of 42 cells/mm^3, a protein concentration of $<$10 mg/dL, and a glucose level of 79 mg/dL. Results of Venereal Disease Research Laboratories testing was negative, and no malignant cells were identified by cytologic examination.

CT of the brain revealed mild left hemispheric mass effect. MR imaging and proton MR spectroscopy were performed on a clinical whole body 1.5-T imaging unit. T2-weighted fast spin-echo (3555/96/1 [TR/effective TE/number of excitations]) and fast FLAIR (7155/112/1; inversion time, 2000 ms) images revealed diffuse hyperintensity involving the left cerebral white matter and basal ganglia, bilateral thalami, and splenium of corpus callosum. Relatively mild mass effect was observed on the left lateral ventricle, and no appreciable enhancement or evidence of necrosis was seen on the T1-weighted images (Fig 1).

Single voxel, water-suppressed spectra were acquired before the IV administration of contrast medium by using a point-resolved spectroscopy (PRESS) sequence (1500/135 [TR/TE]) and a stimulated-echo acquisition mode (STEAM) sequence (1500/20; mixing time, 13 ms), each with 256 accumulations, bandwidth ± 1000 Hz, and 2048 data points. The spectral data were obtained from an 8-mL voxel ($2 \times 2 \times 2$ cm^3) located within the left periatrial area of hyperintensity on the FLAIR images. Single voxel spectra were also obtained from the corresponding contralateral periatrial region by using the same techniques (Fig 2). The spectra shown in Figure 2 were generated by a standard spectral analysis routine, as previously de-

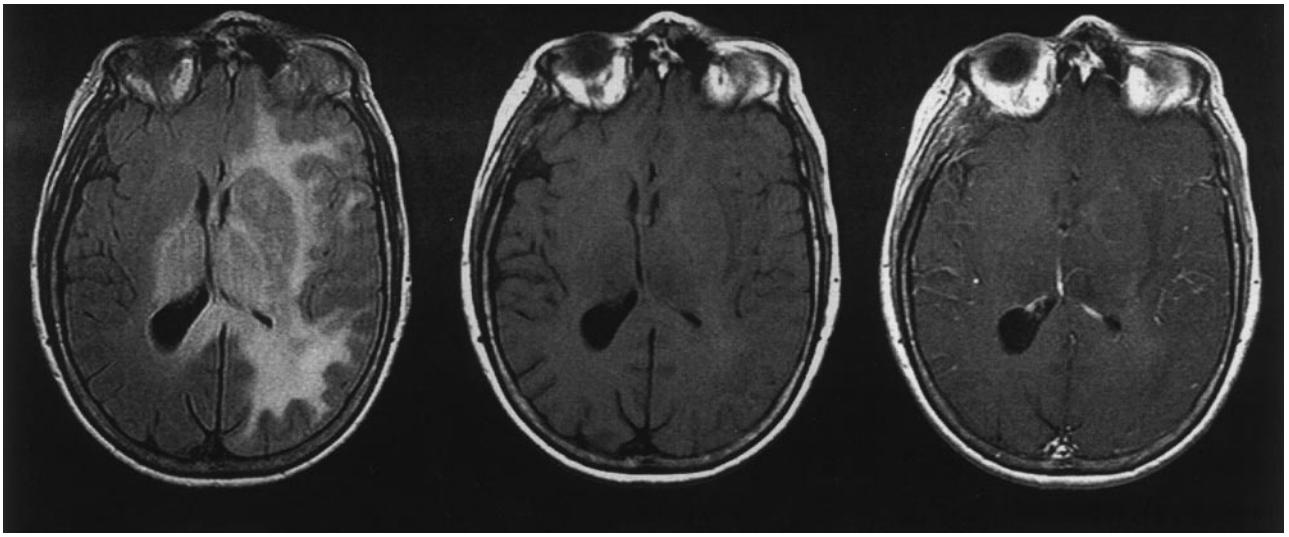

FIG 1. Spin-echo MR images. Axial view FLAIR image (*left*) shows extensive hyperintensity involving the left hemisphere white matter and basal ganglia, bilateral thalami, and splenium of corpus callosum, with mild mass effect. Comparison between unenhanced T1-weighted image (*center*) and contrast-enhanced T1-weighted image (*right*) reveals no appreciable enhancement.

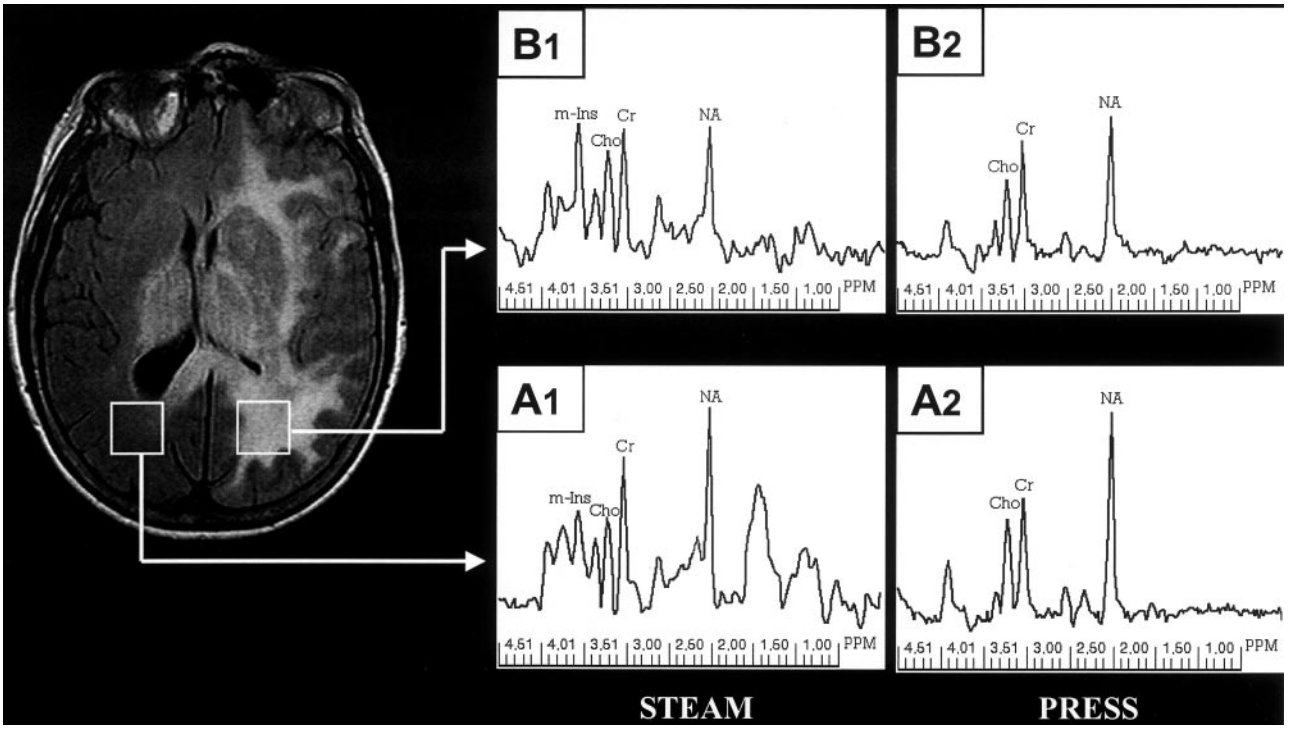

FIG 2. Single voxel spectroscopy. Localized STEAM (TE 20) spectra were acquired from the normal appearing right periatrial region (*A1*) and from the hyperintense left periatrial region (*B1*). PRESS (TE 135) spectra were acquired from the same locations (*A2* and *B2*, respectively). The right and left STEAM spectra are displayed by using the same vertical scale factor, as are the right and left PRESS spectra.

scribed (6). Metabolite concentration ratios were determined by using the LCModel method, also previously described (7). *N*-acetyl (NA), Cho, Cr (at 3.0 ppm), and *m*-Ins (at 3.56 ppm) were determined by fitting the in vivo spectral results with a linear combination of concentration-calibrated, basis-set spectral data in the time domain. The concentration ratios NA/Cr, Cho/Cr, and Cho/NA from STEAM and PRESS spectra and *m*-Ins/Cr and *m*-Ins/NA from STEAM spectra only were calculated for the left and right periatrial regions directly from the individual metabolite concentrations. The concentration ratios for the patient were compared with control data (Table 1) that were obtained in a similar fashion (left hemisphere only) from seven healthy volunteers (mean age ± standard error, 58 ± 5 years) (7).

2D MR spectroscopic imaging was subsequently performed. The 2D section was co-registered with the FLAIR image shown in Figures 1 and 2. Multi-voxel (16×16 array, 18×18 cm^2 region of interest), water-suppressed spectra were acquired before the IV administration of contrast medium by using a PRESS sequence (1500/135, two accumulations, bandwidth ± 1000 Hz, and 2048 data points) with spatial saturation of the outer volume, sparing the central 8×8 array (Fig 3). Each

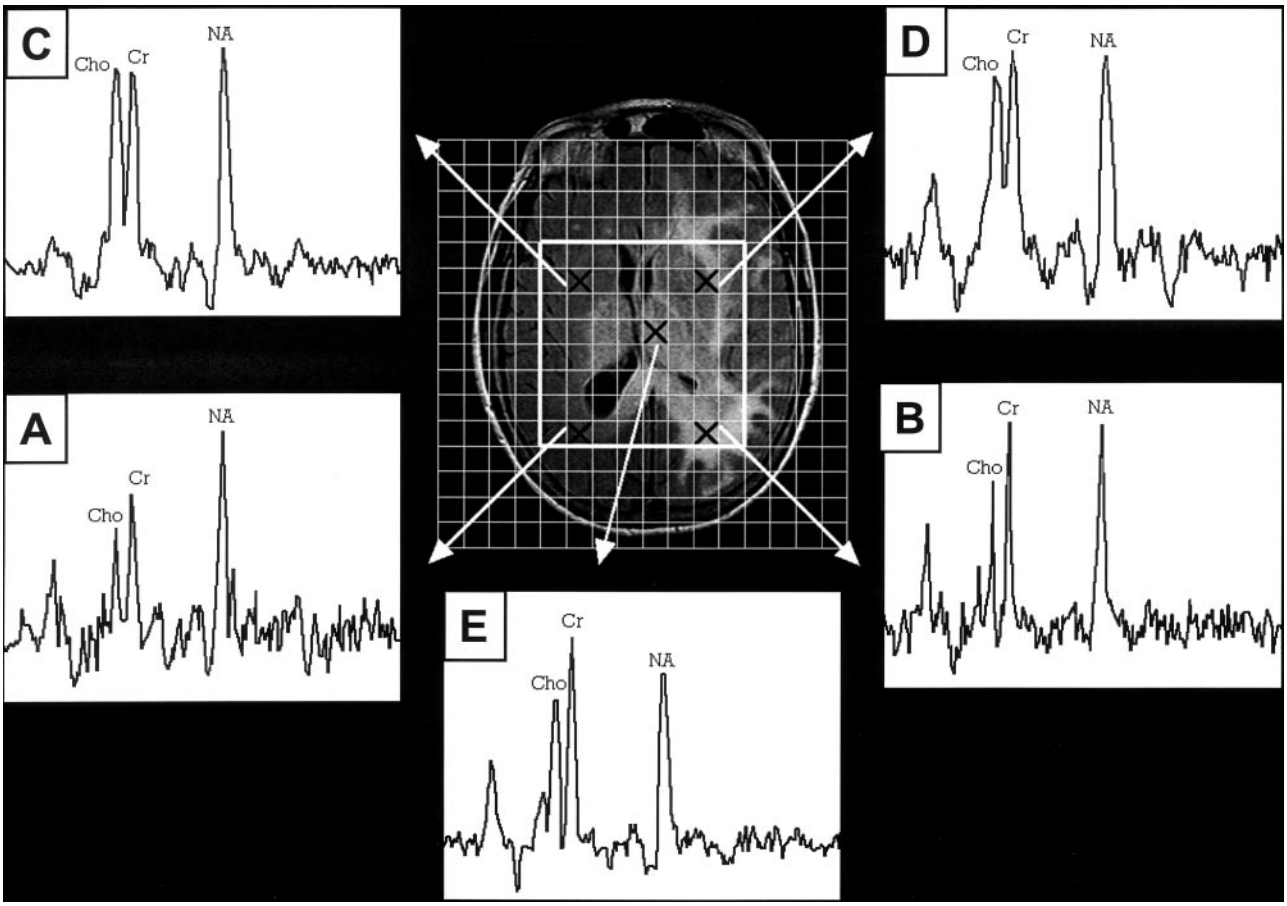

FIG 3. Spectroscopic imaging. Multi-voxel spectra (TE 135) from five different locations (marked by *X*s) indicated on the axial FLAIR localizer. *A*, Right periatrial region. *B*, Left periatrial region. *C*, Right basal ganglia region. *D*, Left basal ganglia region. *E*, Left thalamus.

Table 1. Metabolite concentration ratios from single-voxel MR spectroscopy[α]

	STEAM			PRESS		
Ratio	Left PA[β]	Right PA	Control[γ]	Left PA	Right PA	Control[γ]
NA/Cr	0.81	0.92	1.11 ± 0.12	1.16	1.45	1.61 ± 0.17
Cho/Cr	0.23	0.21	0.17 ± 0.05	0.23	0.25	0.23 ± 0.03
m-Ins/Cr	0.73	0.43	0.46 ± 0.05	nd[δ]	nd	nd
Cho/NA	0.28	0.23	0.15 ± 0.04	0.2	0.18	0.15 ± 0.02
m-Ins/NA	0.9	0.47	0.42 ± 0.04	nd	nd	nd

[α] Metabolite concentration ratios must be multiplied by the ratios of protons contributing to the corresponding resonances in order to obtain "peak area ratios." The ratios for the protons are as follows: NA/Cr = 3/3, Cho/Cr = 9/3, m-Ins/Cr = ~3.4/3, Cho/NA = 9/3, m-Ins/NA = ~3.4/3. Thus, the "peak area ratio" for STEAM, left PA Cho/Cr = 0.23 (9/3) = 0.69. The peak area ratios calculated in this way from the concentration ratios yield results that are qualitatively in agreement with the relative peak areas in Figure 2. If the linewidths of the resonances are not excessively broadened or variable, similar qualitative agreement is achieved when relative peak amplitudes, rather than peak areas, are assessed. {Addendum: The estimate of 3.4 protons contributing to the 3.56-ppm myo-Ins resonance was based on two approaches: (1) analysis of synthetic spectra generated with the TE/TM values used in this case, (2) analysis of metabolite peak area ratios (from a standard peak fitting algorithm) relative to concentration ratios (from LCModel) in a database of 124 similarly acquired control spectra (JB Murdoch, unpublished results).}

[β] PA = periatrial region.

[γ] Control data reported as mean ± standard deviation.

[δ] nd = not determined.

(sub)voxel of the array was approximately 2.5 mL (1.125 × 1.125 × 2 cm^3). The spectra (Fig 3) were generated by using a multi-voxel spectral analysis routine analogous to the one used for single voxel data (6).

For the single voxel STEAM and PRESS spectra, only the left periatrial NA/Cr values were >2 SD below the corresponding mean control values (Table 1). In contrast, neither the left nor the right periatrial Cho/Cr values were >2 SD from the corresponding mean control values. For the STEAM spectra, only the left periatrial *m*-Ins/Cr value was >2 SD above the mean control value. For the PRESS spectra, *m*-Ins was not distinguishable from background noise and could not be determined reliably (Figs 2, *A2* and *B2*, and 3, *A*–*E*).

As shown in Figure 2, the NA, Cho, and Cr amplitudes of the left and right periatrial spectra qualitatively corroborated the data in Table 1. NA relative to Cr was decreased for the left

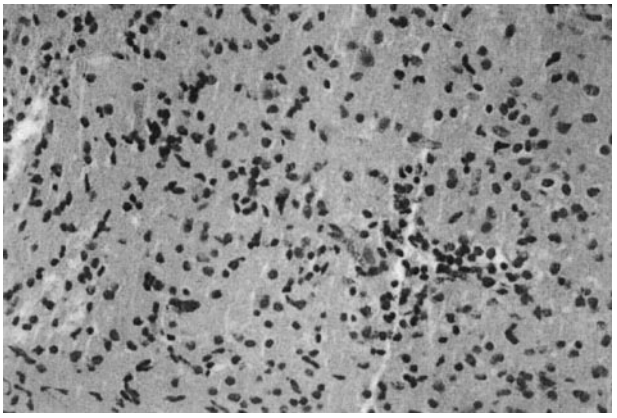

FIG 4. Histopathology of left thalamic biopsy specimen. Moderately cellular infiltrating glioma (hematoxylin and eosin; original magnification, ×400).

periatrial region (Fig 2, *B1* and *B2*) compared with the right periatrial region (Fig 2, *A1* and *A2*). Cho was less than Cr in both periatrial regions on the STEAM (Fig 2, *A1* and *B1*) and PRESS (Fig 2, *A2* and *B2*) spectra. *m*-Ins relative to Cr was markedly increased in the left periatrial region compared with the right periatrial region on the STEAM spectra (Fig 2, *B1* versus *A1*). Uniform vertical scaling for the left versus right STEAM spectra and for the left versus right PRESS spectra made evident the relative decrease in NA and increase in *m*-Ins in the left periatrial region.

The MR spectroscopic imaging results allowed qualitative comparisons between right and left periatrial PRESS spectra (Fig 3, *A* and *B*, respectively) and comparisons with spectra from other locations in the 2D MR spectroscopic imaging grid: basal ganglia spectra (Fig 3, *C* and *D*) and the spectrum from the left thalamus (Fig 3, *E*). For the periatrial spectra (Fig 3, *A* and *B*), the relative peak amplitudes of NA, Cho, and Cr were similar to those shown by the corresponding single voxel spectra (Fig 2, *A2* and *B2*, respectively). The left thalamic spectrum (Fig 3, *E*) was similar in appearance to the left periatrial and basal ganglia spectra (Fig 3, *B* and *D*), showing no elevation of Cho relative to Cr at these diverse locations within the region of abnormal FLAIR signal intensity. LCModel analysis of the left thalamic spectrum yielded NA/Cr = 0.78, Cho/Cr = 0.25, and Cho/NA = 0.31.

A stereotactic biopsy of the left thalamus, using coordinates determined from an MR imaging-compatible frame system, revealed a moderately cellular neoplasm composed of cells with round-to-oval nuclei, some of which displayed small eccentric cell bodies (Fig 4); mitoses were absent. Although glial fibrillary acidic protein immunoreactivity was intense, the small specimen size precluded further interpretation. The lesion was categorized as an infiltrating glioma of intermediate grade (grade II–III when using the WHO classification system, which grades astrocytomas on a scale of I–IV) (1).

Discussion

Gliomatosis cerebri is a rare entity, and the MR imaging findings may be nonspecific, leading to a differential diagnosis that includes neoplastic, inflammatory, and vascular lesions. MR spectroscopy may help narrow the differential diagnosis in favor of a neoplastic lesion by revealing increased Cho/Cr and Cho/NA and variably decreased NA/Cr (2, 3), although, rarely, some nonneoplastic lesions, such encephalitis, demyelinating disease, and organizing hemorrhage, may mimic these spectral changes (8). If Cho/Cr or Cho/NA is not elevated, MR spectroscopy may still help narrow the differential diagnosis in favor of gliomatosis cerebri, based on the findings in this report. Specifically, *m*-Ins/Cr and *m*-Ins/NA should be measured because they can be elevated even when Cho/Cr is normal. To our knowledge, no reports have linked elevated *m*-Ins/Cr and *m*-Ins/NA, determined in vivo, to nonglial, potentially infiltrating neoplasms, such as lymphoma or metastases (11). We are also unaware of any reports documenting normal Cho/Cr and diffusely elevated *m*-Ins/Cr and *m*-Ins/NA in patients with encephalitis, demyelinating disease, or organizing hemorrhage.

As described above, the single voxel proton MR spectroscopy results at TE 20 and TE 135 yielded general agreement between the qualitative appearance of the spectra (Figs 2 and 3) and the metabolite concentration ratios calculated by the LCModel method (Table 1). Although the left periatrial region was not biopsied, the FLAIR and 2D MR spectroscopic imaging results for this region were qualitatively similar to those of the left thalamus, which had proved infiltrating glioma. The left periatrial region hyperintensity shown on FLAIR images is unlikely to be due to edema from localized thalamic tumor because of the following observations. 1) Decreased NA relative to Cr, which was found in the thalamic and left periatrial regions on MR spectroscopic images and confirmed qualitatively and quantitatively (>2 SD from the control mean) for the left periatrial region on single voxel spectroscopy, is a marker for neuronal dysfunction or loss and not edema (9, 10). 2) The right periatrial region exhibited no corresponding hyperintensity despite FLAIR and MR spectroscopic imaging evidence for right thalamic tumor. 3) Edema would not increase metabolite ratios, such as *m*-Ins/Cr, in the left periatrial region. 4) The FLAIR hyperintensity crossing the midline in the splenium of the corpus callosum is typical of tumor spread and not edema (2).

Based on these imaging and spectral findings, the left periatrial region is also involved by gliomatosis cerebri. The finding that is potentially misleading in this case is the normal Cho/Cr ratio. In the series of cases of gliomatosis cerebri reported by Bendszus et al (2) and by Yang et al (3), all cases had elevated Cho/Cr and Cho/NA. Four of the eight cases reported by Bendszus et al, however, were categorized as grade II lesions, and those showed minimal increases in Cho/Cr compared with lesions categorized as grades III and IV.

Although Cho/Cr was not elevated in this case, Cho/NA was abnormally elevated on short TE and borderline on long TE single voxel spectroscopy (Table 1). Thus, results showing elevated Cho/NA should still be considered suspicious for gliomatosis cerebri, even when Cho/Cr is normal. Bendszus et al (2) have recommended that Cho/NA be used to estimate tumor grade and target sites for biopsy.

Compared with controls, *m*-Ins/Cr and *m*-Ins/NA from the short TE single voxel spectrum of the left periatrial region were markedly elevated. Comparing the left periatrial region with the normal appearing

right periatrial region, *m*-Ins/Cr and *m*-Ins/NA exhibited the largest side-to-side differences of any of the metabolite concentration ratios (Table 1). Castillo et al (11) have reported that the *m*-Ins/Cr peak area ratio is significantly greater in low grade (grade II) astrocytoma than in normal brain, anaplastic astrocytoma, and glioblastoma multiforme (in descending order). Based on their results, obtained under single voxel spectroscopy conditions similar to ours (STEAM, TE 20), gliomatosis cerebri in the left periatrial region shows the spectroscopic characteristics of a low grade astrocytoma. Interestingly, the low grade astrocytomas that were reported by Castillo et al (11) had significantly elevated Cho/Cr. The normal Cho/Cr in this case thus sets it apart from the cases of astrocytoma (11) and from most of the cases of gliomatosis cerebri presented by Bendszus et al (2) and Yang et al (3). Because Cho concentrations and Cho/Cr ratios in gliomas are generally considered to reflect membrane lipid turnover accompanying cellular proliferation, the finding of normal Cho/Cr in this case suggests that the tumor cells are not rapidly proliferating, as expected for low histologic grade.

The elevation of *m*-Ins/Cr in low grade astrocytomas is related to the hypothesis that *m*-Ins is a glial marker. Evidence for this hypothesis comes from in vitro MR studies that showed *m*-Ins in perchloric acid extracts of primary cultures of glial cells, C6 glioma cells, and F98 glioma cells but not neuronal cultures (12). The mechanism for the elevation is unclear because of the several roles played by *m*-Ins in cellular metabolism. In one proposed mechanism, the elevation is attributed to changes in the phospholipid composition of glial cell membranes. More specifically, Castillo et al (11) have proposed that mitogen-influenced metabolism of phosphatidyl inositol results in increased phosphatidyl inositol synthesis and corresponding depletion of the MR-visible *m*-Ins pool in high grade astrocytomas and, conversely, decreased phosphatidyl inositol synthesis and corresponding elevation of MR-visible *m*-Ins in low grade astrocytomas. In another, more frequently proposed, mechanism (12), elevation of *m*-Ins is attributed to its action as an organic osmolyte, playing a major role in the volume and osmoregulation of astrocytes; however, the nature of this role in low versus high grade astrocytomas has not been elucidated.

m-Ins and Gly each have resonances in approximately the 3.5 to 3.6 ppm range. In healthy volunteers, a single unresolved peak with a chemical shift at approximately 3.56 (or 3.55) ppm is usually assigned to *m*-Ins, with a small contribution (approximately 10%) from Gly (13). Kinoshita et al (14) have reported, however, that the Gly contribution is elevated in gliomas and that it increases with tumor grade, being greatest in glioblastoma multiforme, based on in vitro high field (6.3 T) spectral data. For in vivo short TE single voxel spectroscopy of suspected glioma at 1.5 T, the relative contributions from *m*-Ins and Gly to a 3.56-ppm peak are not resolved. Thus, in two previous case reports showing normal Cho and an increase in a 3.56-ppm peak on single voxel spectra (TE 30) of gliomatosis cerebri, the peak was assigned to *m*-Ins and/or Gly (4, 5). Long TE spectra, however, can provide evidence of the dominant metabolite, because *m*-Ins exhibits complex J-coupling for spins resonating in the 3.56-ppm region, whereas the α-CH_2 protons of Gly exhibit no coupling effects and have a relatively long T2 relaxation time (15). Thus, the 3.56-ppm peak, which was elevated in the short TE spectra and absent in the long TE spectra of the left periatrial region, was attributed to *m*-Ins.

Additional evidence implicating *m*-Ins is a peak at approximately 3.36 ppm, which appears in all four single-voxel spectra (Fig 2) and in many spectroscopic imaging spectra from the left hemisphere. It corresponds to the singlet resonance of scyllo-inositol. The function of this secondary inositol isomer is unknown, but its concentration generally correlates with that of *m*-Ins at a ratio of 1:12 (16). For this patient, LC-Model analysis of STEAM spectra yielded a scyllo-inositol/Cr ratio of 0.18 in both left and right periatrial regions.

In summary, this case report presents a combination of short and long TE single voxel spectroscopy quantitative results (Fig 2 and Table 1), long TE spectroscopic imaging qualitative results (Fig 3), and FLAIR imaging results for a patient with biopsy-proved infiltrating glioma. The combination of clinical and MR findings is consistent with gliomatosis cerebri yet without elevation of Cho relative to Cr in any region of the lesion, which distinguishes this case from previously reported series of gliomatosis cerebri evaluated with MR spectroscopic imaging (2, 3). The case is distinguished from previous case reports (4, 5) of gliomatosis cerebri with normal Cho because spectroscopic imaging was not used in those reports to document the spatial extent of the normal Cho. Furthermore, the characterization of the 3.56-ppm resonance on short and long TE single voxel spectroscopy in this case provided evidence to support the assignment of this resonance to *m*-Ins rather than Gly, which was not done in the previous articles on gliomatosis cerebri (2–5) or grade II to IV astrocytomas (11). A shortcoming of this study is that a biopsy was not obtained from the left periatrial region, which was sampled by single voxel spectroscopy. Similarities in FLAIR imaging and MR spectroscopic imaging abnormalities for the two regions, however, provided evidence that tumor also infiltrated the left periatrial region. The combination of normal Cho, elevated *m*-Ins, and decreased NA relative to Cr suggests a predominantly low grade lesion (2, 4, 11).

Conclusion

An important corollary to the conclusions reached in this case is that Cho/Cr, which is commonly used in algorithms (along with NA/Cr) to determine the transition zone between regional tumor (elevated Cho/Cr) and edema (normal Cho/Cr) on long TE MR spectroscopic imaging (9), should be interpreted in conjunction with other ratios, such as *m*-Ins/Cr, *m*-Ins/NA, and Cho/NA. Because *m*-Ins is better de-

tected at short TE, both long and short TE MR spectroscopic imaging should be performed. The two sets of spectroscopic imaging data could also be used to approximately estimate the relative contributions of *m*-Ins and Gly to the spectra when tumor is present.

References

1. Kleihues P, Cavanee WK. *WHO Classification of Tumours: Pathology and Genetics of Tumours of the Nervous System.* Lyon: IARC Press; 2000;1–87
2. Bendszus M, Warmuth-Metz M, Klein R, et al. **MR spectroscopy in gliomatosis cerebri.** *AJNR Am J Neuroradiol* 2000;21:375–380
3. Yang S, Wetzel S, Cha S. **Dynamic contrast-enhanced T2*-weighted MR imaging of gliomatosis cerebri.** *AJNR Am J Neuroradiol* 2002;23:350–355
4. Gutowski NJ, Gomez-Anson B, Torpey N, Revesz T, Miller D, Rudge P. **Oligodendroglial gliomatosis cerebri: (1)H-MRS suggests elevated glycine/inositol levels.** *Neuroradiology* 1999;41:650–653
5. Pyhtinen J. **Proton MR spectroscopy in gliomatosis cerebri.** *Neuroradiology* 2000;42:612–615
6. Curless RG, Bowen BC, Pattany PM, Gonik R, Kramer DL. **Magnetic resonance spectroscopy in childhood brainstem tumors.** *Pediatr Neurol* 2002;26:374–378
7. Bowen BC, Pattany PM, Bradley WG, et al. **MR imaging and localized proton spectroscopy of the precentral gyrus in amyotrophic lateral sclerosis.** *AJNR Am J Neuroradiol* 2000;21:647–658
8. Krouwer HG, Kim TA, Rand SD, et al. **Single-voxel proton MR spectroscopy of nonneoplastic brain lesions suggestive of a neoplasm.** *AJNR Am J Neuroradiol* 1998;19:1695–1703
9. Law M, Cha S, Knopp EA, Johnson G, Arnett J, Litt AW. **High-grade gliomas and solitary metastases: differentiation by using perfusion and proton spectroscopic MR imaging.** *Radiology* 2002; 222:715–721
10. Chumas P, Condon B, Oluoch-Olunya D, Griffiths S, Hadley D, Teasdale G. **Early changes in peritumorous oedema and contralateral white matter after dexamethasone: a study using proton magnetic resonance spectroscopy.** *J Neurol Neurosurg Psychiatry* 1997; 62:590–595
11. Castillo M, Smith JK, Kwock L. **Correlation of myo-inositol levels and grading of cerebral astrocytomas.** *AJNR Am J Neuroradiol* 2000;21:1645–1649
12. Brand A, Richter-Landsberg C, Leibfritz D. **Multinuclear NMR studies on the energy metabolism of glial and neuronal cells.** *Dev Neurosci* 1993;15:289–298
13. Kauppinen RA, Williams SR, Busza AL, van Bruggen N. **Applications of magnetic resonance spectroscopy and diffusion-weighted imaging to the study of brain biochemistry and pathology.** *Trends Neurosci* 1993;16:88–95
14. Kinoshita Y, Kajiwara H, Yokota A, Koga Y. **Proton magnetic resonance spectroscopy of brain tumors: an in vitro study.** *Neurosurgery* 1994;35:606–614
15. Mader I, Roser W, Hagberg G, et al. **Proton chemical shift imaging, metabolic maps, and single voxel spectroscopy of glial brain tumors.** *MAGMA* 1996;4:139–150
16. Michaelis T, Helms G, Merboldt KD, Hanicke W, Bruhn H, Frahm J. **Identification of Scyllo-inositol in proton NMR spectra of human brain in vivo.** *NMR Biomed* 1993;6:105–109